East Asian-Australian Monsoon Variations and their Impacts on Regional Climate during Boreal Summer

Wei CHEN

Key Laboratory of Ministry of Education for Meteorological Disaster/International Joint Laboratory on Climate and Environment Change/Collaborative Innovation Center on Forecast and Evaluation of Meteorological Disasters, Nanjing University of Information Science and Technology, China
Meteorology Bureau of Jiangsu Province, China

Zhaoyong GUAN

Key Laboratory of Ministry of Education for Meteorological Disaster/International Joint Laboratory on Climate and Environment Change/Collaborative Innovation Center on Forecast and Evaluation of Meteorological Disasters, Nanjing University of Information Science and Technology, China

Huadong YANG

Key Laboratory of Ministry of Education for Meteorological Disaster/International Joint Laboratory on Climate and Environment Change/Collaborative Innovation Center on Forecast and Evaluation of Meteorological Disasters, Nanjing University of Information Science and Technology, China
Meteorology Bureau of Jiangsu Province, China

and

Qi XU

Meteorology Bureau of Jiangsu Province, China

(Manuscript received 23 April 2019, in final form 18 November 2019)

Abstract

The East Asian summer monsoon (EASM) and the Australian winter monsoon (AWM) are two important components of the Asian−Australian monsoon system during boreal summer. The simultaneous variations of these two monsoons would have remarkable impacts on climate in the Asian−Australian region. Using the reanalysis datasets, we investigated the mechanisms of variation and impacts of East Asian−Australian monsoons (EAAMs). The singular value decomposition (SVD) is performed of the June−July−August (JJA) mean anomalous zonal wind for AWM as the left field and JJA mean anomalous meridional wind for EASM as the right field after both El Niño−Southern Oscillation and India Ocean Dipole signals are filtered out. Our results demonstrate that

Corresponding author: Zhaoyong Guan, Key Laboratory of Ministry of Education for Meteorological Disaster/International Joint Laboratory on Climate and Environment Change/Collaborative Innovation Center on Forecast and Evaluation of Meteorological Disasters, Nanjing University of Information Science and Technology, Nanjing 210044, China
E-mail: guanzy@nuist.edu.cn

AWM and EASM are closely related to each other as revealed by the first leading SVD mode. The anomalously strong (weak) EAAMs correspond to anomalously strong (weak) AWM and EASM to the south of 30°N. When EAAMs are anomalously strong, cold sea surface temperature anomaly (SSTA) appears in regions near northern and northeastern coasts of Australia, whereas the warmer SSTA appears in the northwestern tropical Pacific and South China Sea. The colder SSTA is associated with the upwelling of cold water from below, induced by equatorial easterly anomalies, reinforcing the anticyclonic circulation over Australia through the Matsuno/Gill-type response, whereas warm SSTA appears in the northwestern tropical Pacific and South China Sea as a result of oceanic response to the intensified northwest Pacific subtropical anticyclonic circulation. The EASM couples with AWM via the anomalous easterlies near the equator in the Maritime Continent (MC) region and the slanted vertical anomalous circulations. In the years with strong EAAMs, precipitation decreases in northern Australia and over areas from the western Pacific to Bohai Sea and Yellow Sea of China. Meanwhile, the western MC and the southeastern China experience more-than-normal precipitation.

1.   Introduction

The Asian–Australian monsoon region is located over [40−160°E, 30°S−30°N] (Lau and Wu 1999; Wang et al. 2003) and plays an important role in global climate variations. Weather and climate variations in the Asian–Australian monsoon region are under the control of the South Asian monsoon, the East Asian monsoon, and the Australian monsoon (Meehl 1987; Webster and Yang 1992; Navarra et al. 1999; Kim and Lau 2001; Lau et al. 2005). The East Asian–Australian monsoons (EAAMs) are characterized by rapid seasonal transition. The prevailing East Asian summer monsoon and Australian winter monsoon form the system of East Asian–Australian summer monsoons. Within the longitudinal scope of East Asia–Australia, the climatological East Asian monsoon covers a large longitude span and persists over a long duration. Under the influence of the western Pacific subtropical high (WPSH), the East Asian monsoon displays some subtropical climate features (Chen and Huang 2006, 2007; Zhu et al. 2012). In contrast, the Australian monsoon spans a small range of longitude and only lasts for a short period. In the boreal summer, the Australian winter monsoon (AWM) can affect the East Asian summer monsoon (EASM) via cross-equator flows and subsequently affect weather and climate anomalies in East Asia (Teng et al. 2005; Li and Li 2014).

As important components of the Asian–Australian monsoon circulation system, the East Asian monsoon and Australian monsoon are closely linked with each other (Chen and Guan 2017). Interaction between circulations in the northern and southern hemispheres is realized through the cross-equator flows and their coupling with circulations in the equatorial region (Manton and Mcbride 1992; Matsumoto 1992; Taschetto et al. 2009). Large amounts of air mass and atmospheric moisture as well as energy are transported from the southern hemisphere to the northern hemisphere through the cross-equator flow along 105°E (Simpson 1921; Cong et al. 2007; Jin et al. 2017), which becomes stronger when the EAAMs anomalously intensify (Zhang et al. 2010a, b).

Many factors can affect the East Asia–Australian monsoons. In the upper troposphere, the Asian–Australian dipole (Wang et al. 2016), which mainly depicts the impacts of temperature gradient and circulation in the southern hemisphere, is an important mode in the upper troposphere that strongly affects the Asian–Australian monsoon activities. Meanwhile, the land–sea temperature contrast is the primary influencing factor in the lower troposphere (Wang et al. 2001). In the tropical troposphere, the Asian–Australian monsoon activities are highly correlated with sea surface temperature (SST) in the equatorial Pacific. As an important signal of the interannual variation in air–sea interaction in the equatorial Pacific, ENSO has critical impacts on the Asian–Australian monsoons (Bjerknes 1969; Meehl and Arblaster 1998; Lau and Wu 2001). Since the 1970s, the correlation between ENSO and the Asian–Australian monsoons has been intensifying, which is reflected in the fact that the formation and evolution of ENSO are always accompanied by the

development of westerly anomalies over the Pacific (Wang et al. 2008; Zhu et al. 2012). Zonal wind anomalies in the equatorial region are highly relevant with the EASM and AWM (Chen and Wu 2000; Xu and Chan 2001), suggesting that variations of the EAAMs have crucial influences on the formation and maintenance of ENSO. During ENSO period, cold SST anomalies appear in the western Pacific, which is favorable for the development of circulation anomalies over the subtropical western Pacific and Australia, and thus affect East Asian monsoon anomaly subsequently (Torrence and Webster 1999; Wu and Wang 2002; Wu et al. 2014).

Activities of the EASMs are related to not only SSTA in the western Pacific but also SSTA in the Indian Ocean (Ashok et al. 2001, 2003; Li et al. 2008). The relationship between the Indian Ocean Dipole (IOD), which is one of the most dominant climate variability modes in the Indian Ocean, and anomalies of the Asian–Australian monsoons need to be further investigated (Saji et al. 1999; Li et al. 2003; Meehl et al. 2013). The latent and sensible heat anomalies induced by the IOD can result in anomalous divergence, leading to summer precipitation anomalies of the EAAMs (Saji and Yamagata 2003; Yuan et al. 2008; Jiang et al. 2009; Yu and Guan 2009). During the positive phase of IOD, following the intensification of the Hadley cell, the southeastward cross-equator flow affects the Australian monsoon activities and spatial pattern of precipitation anomaly (Krishnan and Swapna 2009). When a positive IOD event occurs, the cold SST anomaly along with the anomalous anti–cyclonic circulation appears over the eastern Indian Ocean, strengthening the water vapor transport from the Indian Ocean and the Bay of Bengal to eastern China. As a result, more–than–normal precipitation will occur in eastern China (Guan and Yamagata 2003; Zhang et al. 2016).

As aforementioned, the ENSO and IOD are two critical factors that affect the variations of the Asian–Australian monsoons (Guan and Yamagata 2003; Guan et al. 2003). However, the question remains unanswered whether the interaction between the EASM and AWM will change after removing the ENSO and IOD signals. It is also not clear what spatial pattern of climate anomaly is under this situation. As mentioned previously, the East Asian monsoon and Australian monsoon are closely linked via the cross-equator flow over the Maritime Continent (MC) and its coupling with flows in the equatorial region (Ramage 1968; Mcbride et al. 2003; Chang et al. 2005; Xu and Guan 2017a, b). Such an interaction between the northern

and southern hemispheres explains the simultaneous variability in the EASM and the AWM (Chen and Guan 2017), suggesting that climate anomalies in the MC are closely linked with activities of the Asian–Australian monsoons and have great impacts on the monsoon system. Therefore, in the present study, the EASM and AWM are considered as a whole. The aims of the present study are: (1) to explore the various features of the EAAMs after removing the ENSO and IOD signals, (2) to investigate the relationship between the EASM and the AWM, and (3) to reveal the features of climate anomaly in East Asia and Australia.

2. Data and method

The data used in the present study include: (1) the Hadley Center Global SST dataset on 1° × 1° grids (Rayner et al. 2003); (2) the CPC Merged Analysis of Precipitation (CMAP) dataset from the National Oceanic and Atmospheric Administration (NOAA), which is monthly mean precipitation on global 2.5° × 2.5°grids (Schneider et al. 2011); (3) the NCEP/NCAR reanalysis product, which includes monthly mean winds and temperature at 17 pressure levels, vertical velocity at 12 pressure levels, and humidity and surface pressure. The resolution of this dataset is 2.5° × 2.5° (Kalnay et al. 1996); and (4) the GODAS oceanic data (http://ams.confex.com/ams/84Annual/techprogram/paper_70720.htm).

The above data over the period of January 1979–December 2013 are used in the present study. The summer refers to June–July–August (JJA), and the seasons are based on that in the northern hemisphere. Hereafter, the "anomaly" or "deviation" of a variable refers to the difference between the variable and its 35 year average in the summer. The variable is first averaged over the 92 days in each summer, and the result is then averaged over the 35 years.

The MC region is defined as the area over [90–150°E, 10°S–20°N] (Ramage 1968), and the key Maritime Continent region (hereafter KMC) is defined as the area over [95–145°E, 10°S–10°N] (Xu and Guan 2017a, b).

Composite and correlation analyses are implemented in the study. The t-test is applied for significance test of the composite fields and correlations such as wind anomaly. The singular value decomposition (SVD) is used to determine the spatial pattern that is most relevant to the EASM and the AWM.

Multiple regression analysis is conducted. The relevant variable (Y) is regressed onto the JJA mean ENSO index (Niño3.4) and the JJA mean IOD index-

(DMI) to partially remove the effects of ENSO and IOD signals. The regression is expressed as:

$$Y_r = Y - \alpha \times \text{Niño3.4} - \beta \times \text{DMI}, \tag{1}$$

where DMI is defined as the difference between area-averaged SST anomaly over [50−70°E, 10°S−10°N] in the western Indian Ocean and that over [90−110°E, 10°S−equator] in the southeastern Indian Ocean (the former minus the latter). Niño3.4 is defined as the SST anomaly averaged over [170−120°W, 5°S−5°N] in the central eastern Pacific (cf. Saji et al. 1999). Variables α and β are the coefficients of Y regressed onto the ENSO and IOD indices, respectively. Here, the variable Y may be the anomalous rainfall, wind, temperature, etc. Note that the ENSO signal is partially removed from SSTA by regressing SSTA onto Niño3.4 index before the DMI index is calculated. In this way, the quantity Y_r is obtained, which is independent of both ENSO and IOD. Moreover, it is reported that winter ENSO may affect the Indo-western Pacific climate including the Indian Ocean SST during subsequent summer (Xie et al. 2009). However, in the present work, we do not discuss this winter ENSO influences. Instead, we focus on the simultaneous circulation variations. Therefore, the simultaneous multiple regressions in Eq. (1) are used.

The apparent atmospheric heating source Q_1 and apparent water vapor sink Q_2 (Luo and Yanai 1984) are calculated. They are expressed as:

$$Q_1 = C_p \left[\frac{\partial T}{\partial t} + V \cdot \nabla T + \left(\frac{p}{p_0} \right)^k \omega \frac{\partial \theta}{\partial p} \right], \tag{2}$$

$$Q_2 = -L \left(\frac{\partial q}{\partial t} + V \cdot \nabla q + \omega \frac{\partial q}{\partial p} \right). \tag{3}$$

The above algorithms for Q_1 and Q_2 computation include the local change, the horizontal advection, and the vertical transport on the right–hands side of Eqs. (2) and (3). Vertical integrations of algorithms (2) and (3) yield:

$$\langle Q_1 \rangle = \frac{1}{g} \int_{P_T}^{P_S} Q_1 dp = (LP_r + LC - LE) + Q_S + \langle Q_R \rangle, \tag{4}$$

$$\langle Q_2 \rangle = \frac{1}{g} \int_{P_T}^{P_S} Q_2 dp = (LP_r + LC - LE) - LE_S, \tag{5}$$

$$\Delta Q = \langle Q_1 \rangle - \langle Q_2 \rangle = \langle Q_R \rangle + (Q_S + LE_S), \tag{6}$$

where L is the specific latent heat, P_r is the amount of precipitation, Q_S is the surface sensible heat flux, E is the evaporation rate of cloud droplets, E_s is the

evaporation rate at the earth surface, C is the amount of liquid water due to the condensation of water vapor in the column but excluding precipitation, Q_R is the radiative heating rate, $\langle Q_R \rangle$ is the vertically integrated radiative heating (cooling) rate, P_S is the surface pressure, P_T is set to 300 hPa, $\langle Q_1 \rangle$ is the apparent atmospheric heating source, and $\langle Q_2 \rangle$ is the vertically integrated apparent atmospheric water vapor sink. Other symbols are used as conventional.

Note that $\Delta Q = \langle Q_1 \rangle - \langle Q_2 \rangle$, which is the net diabatic heating rate of the atmospheric column except the latent heat release. When the difference between $\langle Q_1 \rangle$ and $\langle Q_2 \rangle$ is very small, it indicates that the water vapor condensation plays a major role for the atmospheric heating. When the difference is positive, it suggests that, in addition to latent heat release, the atmosphere is heated by the net heating of radiative heating, and surface sensible and latent heat fluxes. The opposite is true if the difference is negative. These suggest that ΔQ plays a critical role in the triggering and maintenance of convection.

3. The EAAM anomaly index independent of both ENSO and IOD

The most pronounced feature of the Australian monsoon is the equatorial easterly at 850 hPa and the equatorial westerly at 200 hPa. The zonal wind at 850 hPa averaged over Australia can be used as the index to describe the Australian monsoon variations (Webster 1983; McBride 1987). In contrast, the East Asian monsoon is characterized by distinct alternation of southerly and northerly winds in the summer and winter (Wang and Fan 2013). Thereby, the meridional wind at 850 hPa can be used as the index to depict the East Asian monsoon. Unless otherwise stated, hereafter, the Niño3.4 and IOD signals in the data have been partially filtered out by the regression method as described in Eq. (1).

The zonal wind over [110−160°E, 40−10°S] in Australia is taken as the left field and the meridional wind field over [110−140°E, 20−45°N] in East Asia is taken as the right field for SVD analysis. Results are presented in Table 1 and Fig. 1. After the ENSO and IOD signals are filtered out, the first leading SVD mode accounts for 38.4 % of the total covariance, and the correlation coefficient between time coefficients of the left and right fields can reach up to 0.7, suggesting that the AWM and EASM are closely related to each other. Note that any one of the rest of SVD modes besides SVD1 is also a component of EASM and AWM. But these modes are expected to demonstrate much different features from what the SVD1 does. Hereafter

Table 1.   Statistics of the first two leading SVD modes for analysis of zonal wind in Australia and meridional wind in East Asia at 850 hPa.

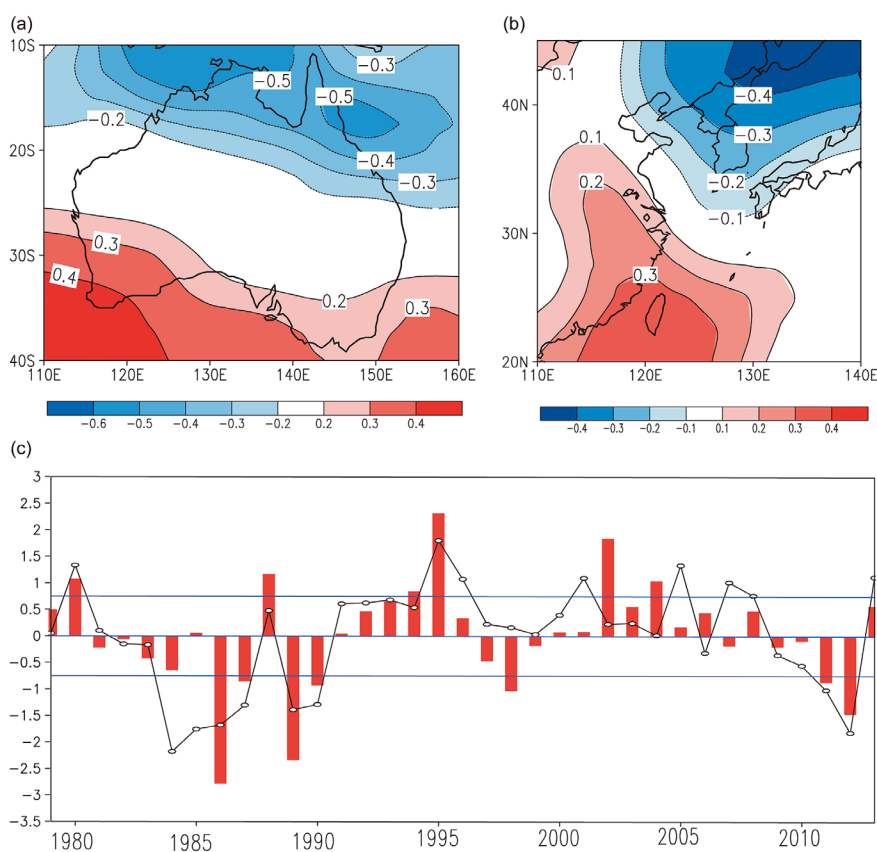| SVD Mode	Covariance explained (%)	Correlation coefficients between time coefficients of the two fields	Variance of the left field explained (%)	Variance of the right field explained (%)
SVD1	38.41	0.70	22.7	11.86
SVD2	27.51	0.50	32.41	11.47

Fig. 1.   Heterogeneous correlation maps (a: left; b: right) of the first leading SVD mode for zonal wind anomaly over Australia (left field) and meridional wind anomaly over East Asia (right field) and their corresponding time series (c) where the red bars (open circled black curve) are for the left (right) field and blue horizontal lines are for values of −0.75, 0.0, and 0.75.

we focus on the analysis of SVD1.

The spatial pattern of the first leading SVD mode (SVD1) of the simultaneous variations of the EAAMs is shown in Fig. 1. It is found that when the winter monsoon is strong in northern Australian (i.e., easterly anomalies occur), positive meridional wind anomalies appear over the East Asia to the south of 30°N with the anomaly center located at the South China Sea to the south of Taiwan Strait. Meanwhile, negative meridional wind anomalies appear to the north of

30°N. The opposite is true when the AWM is weak. Note that Northeast Asia is also the area that is highly correlated with the AWM, which is attributed to the East Asia–Pacific/Pacific–Japan pattern (EAP/PJ) teleconnection induced by the Rossby wave propagation (Huang 1987; Nitta 1987). The high correlation still maintains in East Asia even if the area of the right field is reduced to the south of 35°N.

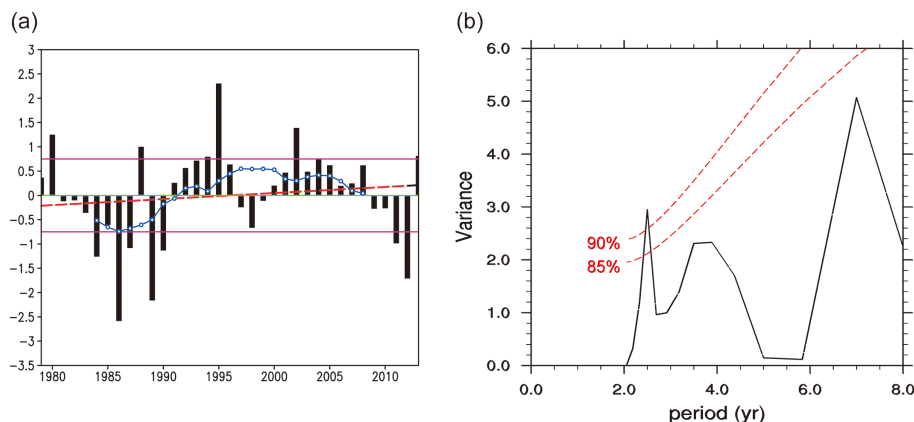Time–series of coefficients of the left and right fields of SVD1 are displayed in Fig. 1c, which shows

Fig. 2. Normalized time series of joint index I^*_{EAA} of the East Asian–Australian monsoon (a) and its global power spectrum (b). The black bars in (a) are for the time series of I^*_{EAA}, the blue curve is for 11-year moving average, and the red dashed straight line is for the linear trend. The horizontal lines in red, green, and red in Fig. 2a are respectively for values of −0.75, 0.0, and 0.75. The red dashed lines in (b) indicate red noise spectrum at the 85 % and 90 % confidence levels, respectively.

distinct interannual variations and the correlation between the two can be up to 0.7. Furthermore, the time coefficients of the left and right fields of SVD1 are averaged and normalized to define the joint index (I^*_{EAA}) of the EASM and the AWM, which is expressed by

$$I^*_{EAA} = TL_{SVD1} + TR_{SVD1}, \qquad (7)$$

where TL_{SVD1} and TR_{SVD1} are the time series of the left and right fields of SVD1, respectively. Note that all data are preprocessed by having the ENSO and IOD signals removed out. According to the definition expressed by the algorithm (7), during boreal summer, a larger positive I^*_{EAA} corresponds to stronger EAAMs, and a larger negative I^*_{EAA} indicates weaker than normal EAAMs. This index tends to describe the relationship that a strong (weak) AWM always corresponds to a strong (weak) EASM.

The EAAMs display obvious interannual and decadal variabilities (Fig. 2). After ENSO and IOD signals are filtered out, a major period of 2−3 years is found to prevail in the EAAM system. Before 1993, the weaker than normal EAAMs were dominant. After 1993, however, the stronger than normal EAAMs are found to be dominant (Wu et al. 2010).

To describe anomalies of the EAAMs, anomalously weak and strong years of the EAAMs are identified based on I^*_{EAA}. The strong years are defined when $I^*_{EAA} \geq 0.75$, and the weak years are determined when $I^*_{EAA} \leqslant -0.75$. In total, there are six strong years and seven weak years, which are listed in Table 2.

Table 2. Strong and weak years of the East Asian–Australian monsoons as identified by using the joint monsoon index I^*_{EAA} during 1979–2013.

Index value	Years
$I^*_{EAA} \geq 0.75$	1980, 1988, 1994, 1995, 2002, 2013
$I^*_{EAA} \leq -0.75$	1986, 1987, 1989, 1990, 2011, 2012

4. Circulation anomalies in East Asian-Australian monsoon region

4.1 Sea level pressure anomalies over Australia and the western Pacific

The Australian High is an important component of the Asian–Australian monsoons (Tao and Chen 1987). Usually, when the anomalous anti–cyclonic circulation occurs over Australia, the AWM strengthens, affecting the cold air activities there. Meanwhile, the northward flow from the equatorial region promotes the establishment of the EASM (Ramage 1968; Hattori et al. 2011; Zhang et al. 2016). In order to explore the relationship between the Australian monsoon anomaly and the Australian High, composite analysis of sea level pressure (SLP) difference between strong and weak EAAM years is conducted. The result is presented in Fig. 3a, which shows that corresponding to strong winter monsoon in northern Australia and equatorial easterly anomalies, SLP in the oceanic area to the southeast of Australia significantly increases with positive SLP anomaly up to 2 hPa from Sidney
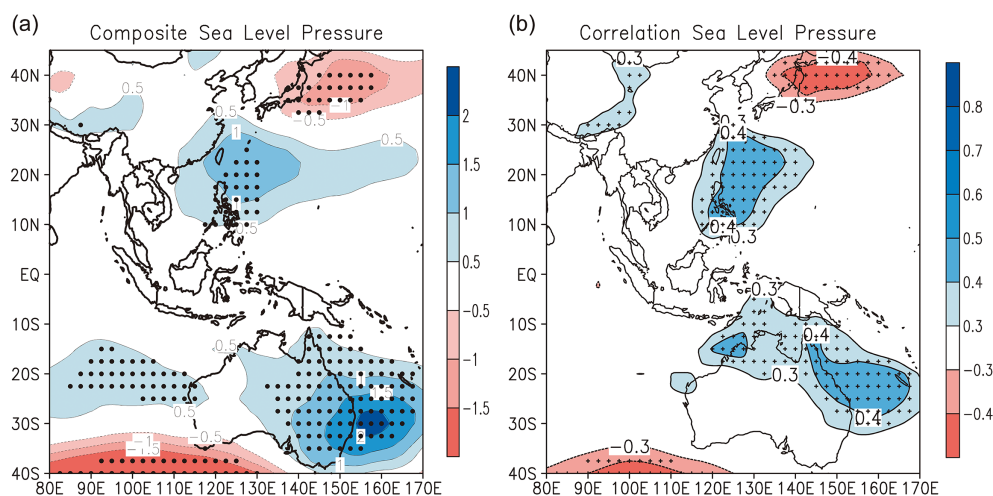
Fig. 3. Composite SLP difference between strong and weak monsoon years after ENSO and IOD signals are removed (a, unit: hPa), and spatial distribution of correlation coefficient between SLP anomalies and the joint index $I*_{EAA}$ of East Asian–Australian monsoons (b). The dotted areas are for values at/above the 95 % confidence level.

to Canberra. This result indicates that the cold Australia High anomalously intensifies. In the northern hemisphere, WPSH also intensifies and high pressure occupies the Philippines and the surrounding area. Meanwhile, SLP decreases in a small area in the midlatitudes to the east of Japan. This circulation pattern is favorable for the intensification of the East Asian monsoon due to the increased pressure gradient force. Moreover, these features can also be observed in correlation distributions (Fig. 3b). The correlation coefficient between SLP anomalies in the northern Australian region and $I*_{EAA}$ can be up to above 0.4 that is statistically significant above the 95 % confidence level. Similarly, the Australian High is positively correlated with $I*_{EAA}$.

Based on the above discussion, it is concluded that corresponding to the positive anomaly of $I*_{EAA}$, the Australian High and the WPSH both intensify, whereas the AWM and EASM also significantly strengthen.

4.2 Horizontal circulation anomalies

When the EAAMs are anomalously strong (Fig. 4a), the region from Australia to the southern Indian ocean is under the control of anticyclonic circulation, which is possibly associated with the effects of negative SST anomalies over MC in northern Australia and the southern Indian Ocean. Note that the strengthened EAAM may also affect the SSTA via wind–evaporation–SST (WES) feedbacks (Xie and Philander 1994) and other possible oceanic dynamical processes. The anomalous divergent air flows from the SPCZ region

intensify the anomalous anticyclonic circulation over Australia in the lower troposphere (Gill 1980; Rodwell and Hoskins 1996). The northern part of the anticyclonic anomaly extends equatorward, leading to easterly anomalies in the equatorial MC region and clock–wise circulation over the Indian Ocean to the north of the equator, where an abnormal anticyclone forms. Meanwhile, a cyclonic anomaly forms around location (160°E, 5°S). Anticyclonic circulation over the western Pacific in the northern hemisphere can also be found, whose genesis is associated with the divergence to its southeast (Gill 1980). The anticyclonic anomalies over Australia and the northwestern Pacific are coupled in the MC, leading to easterly anomalies in this region. Following the intensification of equatorial easterly anomaly at 850 hPa, negative vorticity anomaly in the northern hemisphere and positive vorticity anomaly in the southern hemisphere both become larger (Xie et al. 2008). As a result, the anticyclonic anomalies over the western Pacific and Australia are both strengthened. Note that, the cyclonic anomaly over the northwestern Pacific to the north of 30°N is possibly related to the pole–ward propagation of Rossby waves excited by the near–equatorial forcing (Wang and Rui 1990; Houze et al. 2000).

At 200 hPa in the upper troposphere, the circulation pattern is shown in Fig. 4b. Overall, similar to strong anti–cyclonic anomaly in the lower troposphere above Australia, the anti–cyclonic anomaly also appears in the upper troposphere but shifts slightly southward, demonstrating a barotropic structure over Australia.
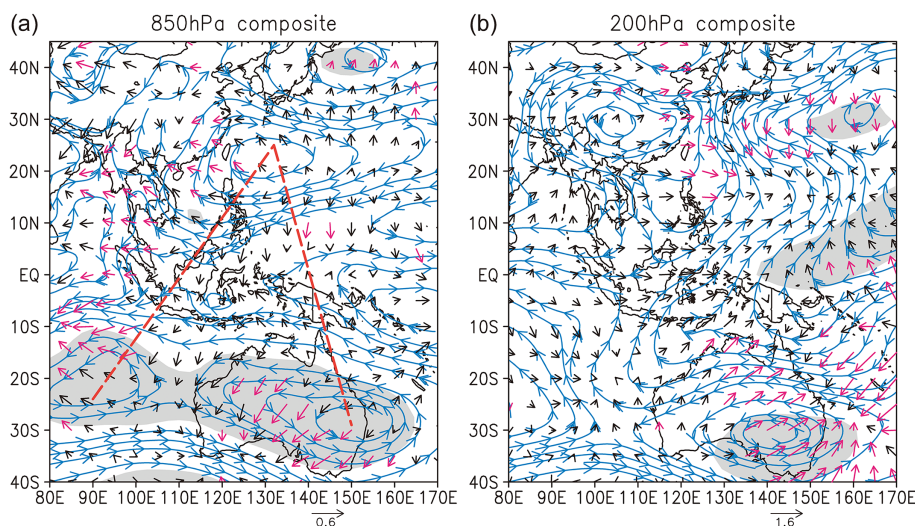
Fig. 4.   Composite differences of horizontal circulations at 850 hPa (a) and 200 hPa (b) between strong and weak
years of East Asian–Australian monsoons after ENSO and IOD signals are filtered out. Blue streamlines are anom-
alies of rotational wind component with shades for values at/above the 95 % confidence level and black arrows for
anomalies of divergent wind component in m s^{-1}. The red arrows indicate the U or V component of the divergent
winds at/above the 95 % confidence level using a *t*-test. The red dashed lines are the routes along which the verti-
cal circulations are plotted as in Fig. 5.

Over the western Pacific, cyclonic circulation at 200
hPa appears in the low-latitude and anticyclonic cir-
culation appears to the north of 30°N. As a whole, the
circulation system shows a baroclinic structure.

4.3   Vertical circulation anomalies

The linkages between EASM and AWM can be
partly exhibited by the vertical circulation anomalies
besides the connections via horizontal circulation
anomalies. As the anomalous anticyclonic circulation
centers are seen respectively over the southwestern
Indian Ocean and the west Australia (Fig. 4a), two
slanted vertical circulations are plotted along the
slanted lines from these two centers to the anomalous
anticyclonic circulation center over the tropical north-
western Pacific, which are presented in Fig. 5 after the
ENSO and IOD signals are filtered out.

The slanted anomalous meridional–vertical circula-
tion from (90°E, 24°S) to (132°E, 25°N) (Fig. 5a) ex-
hibits that, when the AWM is anomalously strong, the
descending motion prevails from northern Australia
northward to equatorial region except for the upward
motion over area around (102°E, 10°S). The slanted
anomalous vertical circulation from (150°E, 29°S) to
(132°E, 25°N) (Fig. 5b) demonstrates a complicated
structure of the anomalous vertical circulation around
(138°E, 7°N). Although the vertical circulations in

Fig. 5 look complicated in some latitudes, the connec-
tions between EASM and AWM link to each other via
these vertical circulations (Wu et al. 2012).

5.   The EAAMs in association with anomalous thermal forcing

5.1   SST anomaly

Theoretically, the warmer–than–normal SST in the
northwestern tropical Pacific may force the atmo-
sphere to respond, inducing an anomalous cyclonic
circulation to its northwest (Gill 1980). On the other
hand, the warmer–than–normal SST may also be a
result of the oceanic response to the surface fluxes of
momentum and radiative forcings. Overall, when the
EAAMs are stronger than normal, pronounced warm
SSTA appears to the east of 150°E in the equatorial
western Pacific (Fig. 6), whereas cold SSTA occurs
between 120°E and 150°E near the equator.

In the northwestern tropical Pacific, the anomalous
anticyclonic circulation occupies that region, suggest-
ing that the warmer SSTA in northwestern tropical Pa-
cific is possibly a result of the anomalous anticyclone.
Because of Coriolis force, this anomalous anticyclone
forces the warmer water to converge into its center
part and henceforth to result in down–welling there
(not shown), leading to the underlying ocean surface
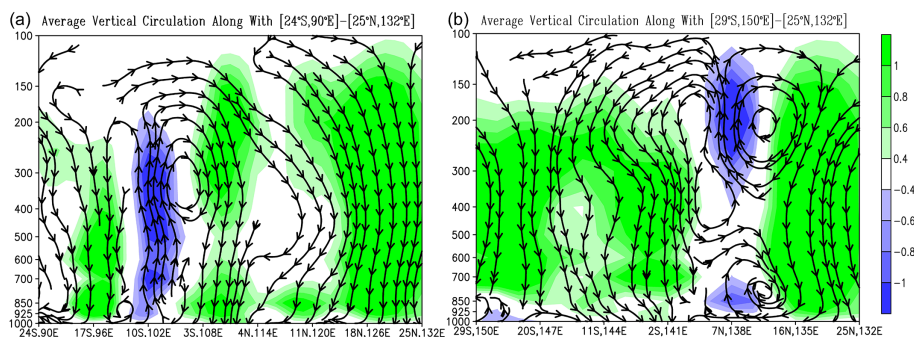to be warmer than normal. Besides, because of the air

Fig. 5.   Composite differences of vertical circulations between strong and weak monsoon years along the red dashed lines in Fig. 4a. Shown in (a) are the slanted vertical circulation anomaly along with the line from (90°E, 24°S) to (132°E, 25°N) whereas in (b) the slanted vertical circulation from (15°E, 29°S) to (132°E, 25°N). The vertical velocity anomalies (in × 10^{-2} hPa s^{-1}) are shaded.
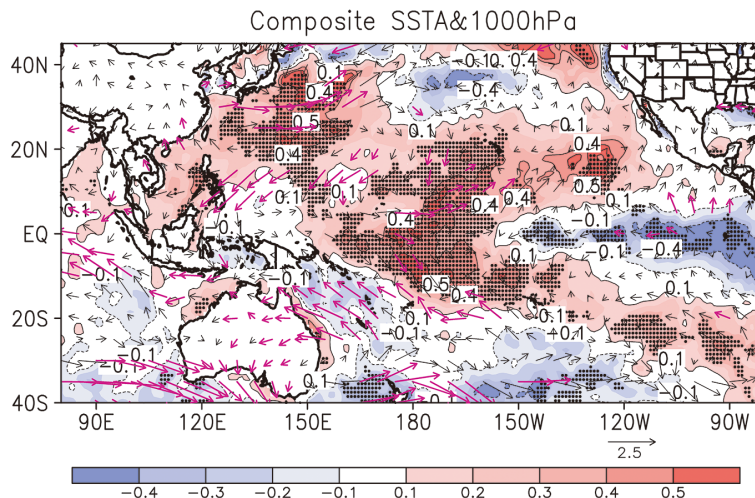

Fig. 6.   Composite difference of SST anomalies between strong and weak EAAM years after the ENSO and IOD signals are filtered out. The contours are for the differences of SSTA (°C) with stippled areas for values at/above the 95 % confidence level. Arrows are for surface wind anomalies (m s^{-1}) at 1000 hPa with red arrows for U or V component significant at/above the 95 % confidence level.

downdraft in the anomalous anticyclonic circulation (Fig. 5a), the solar radiation near the ocean surface there may be stronger than normal (not shown), leading to the ocean to absorb more solar radiations and hence resulting in higher–than–normal SSTA there. In the South China Sea, warm ocean water converges there because of the effect of anomalous sea surface wind stress, and the more–than–normal solar radiation absorption also occurs there.

Anomalous atmospheric thermal forcing induced by SSTA can result in distinct circulation anomaly in tropical region via the Matsuno/Gill-type response

(Matsuno 1966; Gill 1980). The cold SSTA in the eastern MC is related to the upwelling of cold ocean water induced by the equatorial easterly anomaly (not shown). Of course, the evaporation rate in this area is also found to be larger than normal (not shown), which is favorable for SST to be colder than normal. As shown in Fig. 6, the act of easterly anomalies on the ocean surface produces poleward Coriolis force, which subsequently induces divergence of ocean water on the surface and upwelling of cold ocean water from below. Using the GODAS oceanic data, we have performed the composite analysis of the vertical velocity
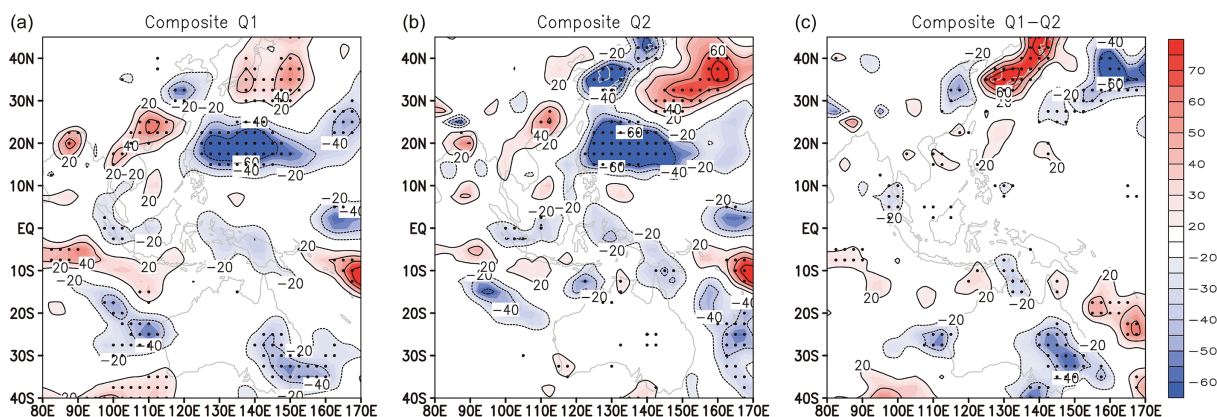
Fig. 7. Composite difference of anomalous apparent heating source $\langle Q_1 \rangle$ (a), anomalous apparent water vapor sink $\langle Q_2 \rangle$ (b), and net diabatic heating anomalies $\Delta Q = \langle Q_1 \rangle - \langle Q_2 \rangle$ (W m^{-2}) (c). Stippled areas are for values at/above the 95 % confidence level.

at 10m depth averaged over area [120−150°E, 10°S−equator] between strong and weak EAAM years. It is found that the anomalous vertical velocity is 1.54×10^{-6} m s^{-1}, indicating that there does exist the anomalous upwelling in this region. Meanwhile, the cold SSTA results in lower atmosphere cooling and divergence (Fig. 4a), which is favorable for evaporation in the ocean surface (not shown). The WES feedback loop actually maintains the cold SSTA (Xie and Philander 1994). Warm SSTA is dominant in the northern Indian Ocean, and cold SSTA is dominant in the southern Indian Ocean, which are respectively associated with the anomalous anticyclonic circulations on both sides of the equatorial Indian Ocean.

It is noted that the SSTA pattern as shown in Fig. 6 looks like the Central Pacific type SSTA pattern, which is considered as an SSTA mode independent of canonical ENSO (Ashok et al. 2007; Kao and Yu 2009; Kug et al. 2009; Wang et al. 2018). The EAAMs may be partly influenced by Central–Pacific–type SSTA pattern.

5.2 Thermal forcing anomaly

Although the SSTA can lead to anomalous atmospheric thermal forcing and vice versa, it is still not clear whether the atmosphere above the warmer SSTA area is heated or not. Hence, in Fig. 7, the anomalous diabatic heatings derived from reanalysis in terms of Eqs. (4)−(6) are presented.

Corresponding to anomalous EAAMs, there exist significant atmospheric heating anomalies. When the EAAMs are stronger than normal, negative apparent heating $\langle Q_1 \rangle$ appears in the eastern MC and from the

southern Indian Ocean to southern Australia (Fig. 7a), which is attributed to less latent heat release caused by anomalous descending motions in these areas (Fig. 7b) and weak net radiative cooling in the atmospheric column (Fig. 7c). Meanwhile, negative apparent water vapor sink anomalies are largely distributed over the Indian Ocean and extend eastward to the coastal region of northern Australia, which are associated with the cold SSTA in this region (Fig. 6). In the northern hemisphere, large areas of negative $\langle Q_1 \rangle$ and $\langle Q_2 \rangle$ anomalies appear in the western Pacific and Bohai Sea and Yellow Sea of China. The negative center is located at around 20°N. These anomalous diabatic coolings facilitate the intensification of the anticyclonic circulation over the northwestern tropical Pacific. Over Japan and the Pacific ocean to the east of Japan, $\langle Q_1 \rangle$ and $\langle Q_2 \rangle$ anomalies are positive (significant at the 95 % confidence level); the positive $\langle Q_1 \rangle$ anomaly center is located in region south of the middle and lower reaches of the Yangtze River with the value of up to above 60 w m^2, implying positive precipitation anomaly in this region (Fig. 8a).

Note that to the east of 120°E, the spatial distribution of apparent heating source and apparent water vapor sink anomalies displays a "+ − +" pattern from region east of the Philippines northeastward to the mid- and high-latitude regions in both the $\langle Q_1 \rangle$ and $\langle Q_2 \rangle$ anomalies. This result indicates that the circulation anomalies in the northern hemisphere might be affected by the EAP/PJ teleconnection pattern (Huang 1987; Nitta 1987).

The diabatic heating anomalies mentioned above, especially those in the equatorial region induced by
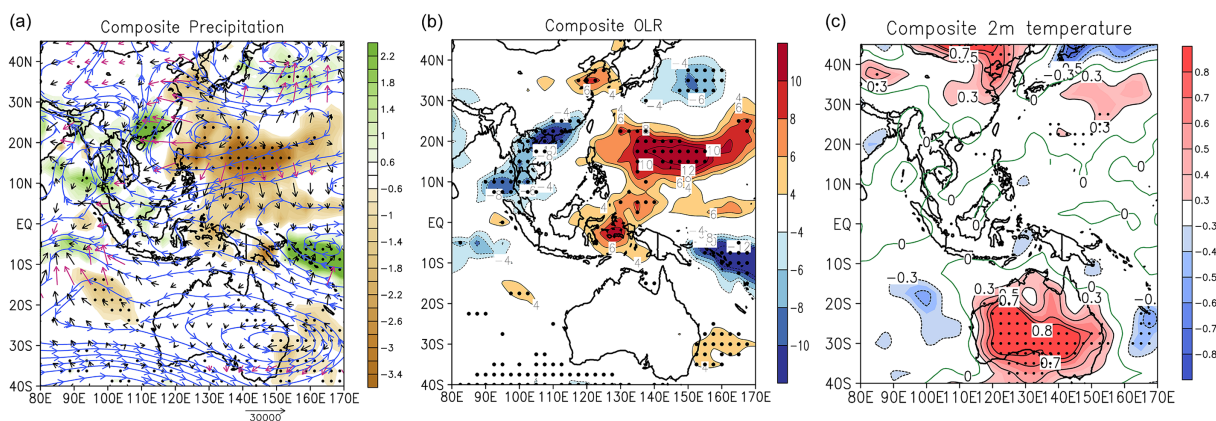
Fig. 8. Composite differences of precipitation, OLR, and 2 m temperature between strong and weak East Asian–Australian monsoons years after ENSO and IOD signals are filtered out. Shaded areas in (a) indicate precipitation anomaly (mm d^{-1}). Streamlines indicate the rotational component of the whole layer of water vapor flux anomaly (10^{-6} g s^{-1} cm^{-2}) integrated from 1000 to 300 hPa with red arrows for the U or V component at/above the 95 % confidence level. Shaded areas in (b) indicate OLR anomaly (W m^{-2}), and shaded areas in (c) denote 2 m temperature anomaly (°C). The stippled areas are for values at/above the 95 % confidence level.

SSTA, can definitely cause tropical circulation anomalies via the Gill-type response (Fig. 4). Through wave trains that propagate meridionally, these tropical circulation anomalies can subsequently affect atmospheric circulation in higher latitudes and result in abnormal monsoon activities over the East Asia–Australia region.

6. Climate anomalies in the East Asian-Australian monsoon region

As the carrier of water vapor transport, the monsoon circulation plays a key role in regulating the precipitation variations in EAAM regions (Chen and Pfaendtner 1993; Ding and Chan 2005; Yang et al. 2007). Extremely anomalous high and low precipitation can lead to disastrous flooding and droughts over large areas, causing severe economic loss in these monsoon regions. Composite differences of precipitation and water vapor flux divergence between high and low I^*_{EAA} years are presented in Fig. 8 for understanding the impacts of AWM anomalies on regional precipitation.

In the years with strong AWM (Fig. 8a), precipitation greatly decreases in southeastern Australia and some areas in the southern Indian Ocean. In the northern hemisphere, less than normal precipitation appears over large areas in the tropical northwestern Pacific, which is found to be less than −3.4 mm d^{-1} (above 95 % confidence level) between high and low I^*_{EAA} years. Such a large precipitation anomaly is mainly associated with water vapor divergence there, which is

a result of the anomalous anticyclonic circulation over the northwestern tropical Pacific (Fig. 4a).

In contrast, precipitation is more than normal in the equatorial Pacific to the east of 150°E, which is related to the water vapor transport near the SPCZ in the southwestern Pacific (Fig. 8a). It can also be seen that precipitation significantly increases from the western MC and northern Indian Ocean to Grand Sunda Islands, which is attributed to significant atmospheric moisture convergence over a small area in the equatorial Indian Ocean. It should be emphasized that more precipitation is observed over a narrow belt extending from the coastal region of southeastern China. This is due to the lower tropospheric convergence of the anomalous southerly winds from Indochina region and southerly winds from east part of South China Sea along the west flank of the anomalous anticyclonic circulation over the northwestern tropical Pacific. Also, more precipitation is received over anomalous regions east of Japan, where the water vapor converges from the north flank of the same anomalous anticyclonic circulation over the northwestern Pacific.

The outgoing longwave radiation (OLR) correspondingly changes when the SST and convections change. Apparently, high OLR is found over weak convection region with less precipitation whereas low OLR is observed over region where more–than–normal precipitation is observed (Fig. 8b). When the AWM is anomalously strong, OLR is slightly lower than normal in eastern Australia and the equatorial

Indian Ocean. In the northern hemisphere, OLR is significantly lower than normal over the area that extends southeastward from the northwestern MC to the coastal region of southeastern China and the Pacific Ocean to the east of Japan, where strong convective activities result in large amounts of precipitation. Large areas of high OLR with differences up to more than 12 W m^{-2} between high and low I^*_{EAA} years are found over the New Guinea, the western Pacific near 20°N, and Bohai Sea and Yellow Sea of China, where convection is weak and precipitation is less than normal.

The EAAMs differ during high and low I^*_{EAA} years, affecting the surface air temperatures in East Asian and Australian regions. Because the influences of anticyclonic anomalies (Fig. 4a) over Australia and the northwestern Pacific, warm temperature anomalies occur over large areas of the above regions, especially over Australia with up to 0.8°C there (Fig. 8c). Over the northeastern China and northwestern Pacific, the higher–than–normal temperatures are also found (Fig. 8c). Both regions are affected by the southerly winds from the west and north flanks of the anomalous anticyclonic circulation over the northwestern Pacific (Fig. 4a). In contrast, 2 m air temperature is anomalously low though small in the equatorial region, which is partially attributed to the effects of equatorial easterly anomalies. The easterly anomalies induce poleward Coriolis force and upwelling of cold water from below, leading to anomalously cold SST and atmospheric cooling (Fig. 6). Of course, solar radiation that can reach the surface decreases when precipitation is more than normal, which also induces the surface air temperature to be lower than normal.

7. Summary and discussion

In the present study, the anomalies of the EAAMs after ENSO and IOD signals are filtered out are investigated by employing the SVD analysis method. It is found that the correlation coefficient between left and right fields of the first leading SVD mode (SVD1) is up to 0.7, suggesting that the AWM and the EASM are closely related with each other. Further analysis of SVD1 is conducted and the joint EAAMs index I^*_{EAA} is defined. Major conclusions are as follows.

Anomalies of the AWM and the EASM can occur simultaneously. When the AWM is anomalously strong, the cold Australian High and the WPSH both intensify and the EASM becomes stronger to the south of 30°N. Such simultaneous changes of the monsoons and related circulation systems are associated with SST anomalies in the equatorial Pacific.

Corresponding to the stronger than normal EAAMs,

pronounced cold SSTA occurs over northern and northeastern Australian coastal regions. The cold SSTA is possibly associated with the upwelling of deep, colder water induced by equatorial easterly anomalies and leads to atmospheric cooling in the lower level of troposphere. Via the Matsuno/Gill-type response, an anomalous anticyclonic circulation is induced at 850 hPa above Australia, further intensifying the Australian High. Over the northwestern tropical Pacific, the atmospheric diabatic cooling in the lower troposphere results in intensification of the WPSH. The SSTAs are significantly warmer in the northwestern tropical Pacific, attributed to anomalous anticyclonic circulation there, where more solar radiation reaches the ocean surface and sea surface water anomalously converges.

Anomalies of the EAAMs have distinct impacts on regional climate in the monsoon region. When the EAAMs are stronger than normal, precipitation tends to decrease over northern Australia and from the western Pacific to Bohai Sea and Yellow Sea of China; meanwhile, the western MC and the southeastern China would experience more precipitation and warmer surface air temperature. Cold surface air temperature anomalies are largely found in the area from the southern Indian Ocean to the equatorial region.

Recently, we concluded that the EAAMs may vary concurrently (Chen and Guan 2017). In the present study, although both ENSO and IOD signals are removed out from all the data we used, the results are still in consistent with those as reported in Chen and Guan (2017); the anomalous anticyclonic circulations above Australia and the western Pacific couple with each other over the MC, leading to the formation of equatorial easterly anomalies in this region. The anticyclonic anomalies in the northern and southern hemispheres are linked to each other through the equatorial easterly anomalies in the present study.

Note that the EAAMs may interact with the ocean in the Asian–Australian monsoon regions. The SSTA may have impacts on the EAAMs as displayed in Figs. 4–6, inducing the EAAMs to vary anomalously. On the other hand, the strengthened EAAMs may also affect the SSTA via wind–evaporation–SST (WES) feedbacks (Xie and Philander 1994) and other possible oceanic dynamical processes. These need to be investigated in more detail in the future. The EAAMs look to vary with a periodicity of 2–3 years, but the formation of the 2–3 years period is still unclear. Moreover, the reasons why WPSH changes are also not clear. These puzzles deserve further examining. Besides of these issues, it is also noted that variations of the Asian–Australian monsoons are significantly

affected by ENSO and IOD (Ashok et al. 2003; Guan and Yamagata 2003; Wang et al. 2008; Jourdain et al. 2013). What and how the ENSO and IOD as well as the SSTA in other oceanic regions affect the co-variations of EAAMs are still not so clear. The further examinations using the general circulation models are needed in the near future.

Acknowledgements

References

Ashok, K., Z. Guan, and T. Yamagata, 2001: Impact of the Indian Ocean dipole on the relationship between the Indian monsoon rainfall and ENSO. *Geophys. Res. Lett.*, **23**, 4499–4502.

Ashok, K., Z. Guan, and T. Yamagata, 2003: Influence of the Indian Ocean Dipole on the Australian winter rainfall. *Geophys. Res. Lett.*, **30**, 1821, doi:10.1029/2003GL 017926.

Ashok, K., S. K. Behera, S. A. Rao, H. Weng, and T. Yamagata, 2007: El Niño Modoki and its possible teleconnection. *J. Geophys. Res.*, **112**, C11007, doi:10.1029/2006JC003798.

Bjerknes, J., 1969: Atmosphere teleconnections from the equatorial pacific. *Mon. Wea. Rev.*, **97**, 163–172.

Bo, Y., and C.-H. Wang, 2016: The mechanism of thickness of geopotential height diploe and its relation with climate variability in Asia-Australia in boreal winter. *J. Trop. Meteor.*, **32**, 85–93 (in Chinese).

Chang, C.-P., Z. Wang, J. McBride, and C.-H. Liu, 2005: Annual cycle of Southeast Asia—Maritime Continent rainfall and the asymmetric monsoon transition. *J. Climate*, **18**, 287–301.

Chen, J.-H., and R.-H. Huang, 2006: The comparison of climatological characteristics among Asian and Australian monsoon subsystems. Part I. The wind structure of summer monsoon. *Chin. J. Atmos. Sci.*, **30**, 1091–1102 (in Chinese).

Chen, J.-H., and R.-H. Huang, 2007: The comparison of climatological characteristics among Asian and Australian monsoon subsystems. Part II: Water vapor transport by summer monsoon. *Chin. J. Atmos. Sci.*, **31**, 766–778 (in Chinese).

Chen, L., and R. Wu, 2000: The role of the Asian/Australian monsoons and the Southern/Northern Oscillation in the ENSO cycle. *Theor. Appl. Climatol.*, **65**, 37–47.

Chen, T.-C., and J. Pfaendtner, 1993: On the atmospheric branch of the hydrological cycle. *J. Climate*, **6**, 161–167

Chen, W., and Z. Y. Guan, 2017: A joint monsoon index for East Asian–Australian monsoons during boreal summer. *Atmos. Sci. Lett.*, **18**, 403–408.

Cong, J., Z.-Y, Guan, and L.-J. Wang, 2007: Interannual (interdecadal) variabilities of two cross-equatorial flows in association with the Asia summer monsoon variations. *J. Nanjing Inst. Meteor.*, **30**, 779–785 (in Chinese).

Ding, Y., and C. J. Chan, 2005: The East Asian summer monsoon: An overview. *Meteorol. Atmos. Phys.*, **89**, 117–142.

Gill, A., 1980: Some simple solutions for heat-induced tropical circulation. *Quart. J. Roy. Meteor. Soc.*, **106**, 447–462.

Guan, Z., and T. Yamagata, 2003: The unusual summer of 1994 in East Asia: IOD teleconnections. *Geophys. Res. Lett.*, **30**, 1544, doi:10.1029/2002GL016831.

Guan, Z., K. Ashok, and T. Yamagata, 2003: Summertime response of the tropical atmosphere to the Indian Ocean Dipole sea surface temperature anomalies. *J. Meteor. Soc. Japan*, **81**, 533–561.

Hattori, M., S. Mori, and J. Matsumoto, 2011: The cross-equatorial northerly surge over the Maritime Continent and its relationship to precipitation patterns. *J. Meteor. Soc. Japan*, **89**, 27–47.

Houze, R. A., Jr., S. S. Chen, D. E. Kingsmill, Y. Serra, and S. E. Yuter, 2000: Convection over the Pacific warm pool in relation to the atmospheric Kelvin-Rossby wave. *J. Atmos. Sci.*, **57**, 3058–3089.

Huang, R. H., 1987: Influence of the heat source anomaly over the tropical western Pacific on the subtropical high over East Asia. *Proceedings of the International Conference on the General Circulation of East Asia*, Chengdu, China, Chinese Academy of Sciences, 40–51.

Jiang, L., Z. Guan, C. Lu, and D. Qian, 2009: Interdecadal characters of relationships of the interannual variability of East Asian summer monsoon with IOD and ENSO. *Trans. Atmos. Sci.*, **32**, 32–44 (in Chinese).

Jin, D., Z. Guan, L. Huo, and X. Wang, 2017: Possible impacts of spring sea surface temperature anomalies over South Indian Ocean on summer rainfall in Guangdong-Guangxi region of china. *Climate Dyn.*, **49**, 3075–3090.

Jourdain, N. C., A. S. Gupta, A. S. Taschetto, C. C. Ummenhofer, A. F. Moise, and K. Ashok, 2013: The Indo-Australian monsoon and its relationship to ENSO and IOD in reanalysis data and the CMIP3/CMIP5 simulations. *Climate Dyn.*, **41**, 3073–3102.

Kalnay, E., M. Kanamitsu, R. Kistler, W. Collins, D. Deaven, L. Gandin, M. Iredell, S. Saha, G. White, J. Woollen, Y. Zhu, M. Chelliah, W. Ebisuzaki, W. Higgins, J. Janowiak, K. C. Mo, C. Ropelewski, J. Wang,

A. Leetmaa, R. Reynolds, R. Jenne, and D. Joseph, 1996: The NCEP/NCAR 40-Year Reanalysis project. *Bull. Amer. Meteor. Soc.*, **77**, 437–471.

Kao, H.-Y., and J.-Y. Yu, 2009: Contrasting eastern-Pacific and central-Pacific types of ENSO. *J. Climate*, **22**, 615–632.

Kim, K.-M., and K.-M. Lau, 2001: Dynamics of monsoon–induced biennial variability in ENSO. *Geophys. Res. Lett.*, **28**, 315–318.

Krishnan, R., and P. Swapna, 2009: Significant influence of the boreal summer monsoon flow on the Indian Ocean response during dipole events. *J. Climate*, **22**, 5611–5634.

Kug, J.-S., F.-F. Jin, and S.-I. An, 2009: Two types of El Niño events: Cold tongue El Niño and warm pool El Niño. *J. Climate*., **22**, 1499–1515.

Lau, K. M., and H.-T. Wu, 1999: Assessment of the impacts of the 1997–98 El Niño on the Asian–Australia monsoon. *Geophys. Res. Lett.*, **26**, 1747–1750.

Lau, K.-M., and H.-T. Wu, 2001: Principal modes of rainfall–SST variability of the Asian summer monsoon: A reassessment of the monsoon–ENSO relationship. *J. Climate*, **14**, 2880–2895.

Lau, N.-C., A. Leetmaa, M. J. Nath, and H.-L. Wang, 2005: Influences of ENSO-induced Indo–western Pacific SST anomalies on extratropical atmospheric variability during the boreal summer. *J. Climate*, **18**, 2922–2942.

Li, C., and S. Li, 2014: Interannual seesaw between the Somali and the Australian cross-equatorial flows and its connection to the East Asian summer monsoon. *J. Climate*, **27**, 3966–3981.

Li, S., J. Lu, G. Huang, and K. Hu, 2008: Tropical Indian Ocean basin warming and East Asian summer monsoon: A multiple AGCM study. *J. Climate*, **21**, 6080–6088.

Li, T., B. Wang, C.-P. Chang, and Y. Zhang, 2003: A theory for the Indian Ocean dipole–zonal mode. *J. Atmos. Sci.*, **60**, 2119–2135.

Luo, H., and M. Yanai, 1984: The large-scale circulation and heat sources over the Tibetan Plateau and surrounding areas during the early summer of 1979. Part II: Heat and moisture budgets. *Mon. Wea. Rev.*, **112**, 966–989.

Manton, M. J., and J. L. Mcbride, 1992: Recent research on the Australian monsoon. *J. Meteor. Soc. Japan*, **70**, 275–285.

Matsumoto, J., 1992: The seasonal changes in Asian and Australian monsoon regions. *J. Meteor. Soc. Japan*, **70**, 257–273.

Matsuno, T., 1966: Quasi-geostrophic motions in the equatorial area. *J. Meteor. Soc. Japan*, **44**, 25–43.

McBride, J. L., 1987: The Australian summer monsoon. *Monsoon Meteorology*, Chang, C.-P., and T. N. Krishnamurti (eds.), Oxford University Press, 203–231.

McBride, J. L., M. R. Haylock, and N. Nicholls, 2003: Relationships between the Maritime Continent heat source

and the El Niño–Southern Oscillation phenomenon. *J. Climate*, **16**, 2905–2914.

Meehl, G. A., 1987: The annual cycle and interannual variability in the tropical Pacific and Indian Ocean regions. *Mon. Wea. Rev.*, **115**, 27–50.

Meehl, G. A., and J. M. Arblaster, 1998, The Asian–Australian monsoon and El Niño–Southern Oscillation in the NCAR climate system model. *J. Climate*, **11**, 1356–1385.

Meehl, G. A., A. Hu, J. M. Arblaster, J. Fasullo, and K. E. Trenberth, 2013: Externally forced and internally generated decadal climate variability associated with the interdecadal Pacific oscillation. *J. Climate*, **26**, 7298–7310.

Navarra, A., M. N. Ward, and K. Miyakoda, 1999: Tropical–wide teleconnection and oscillation. I: Teleconnection indices and type I/type II states. *Quart. J. Roy. Meteor. Soc.*, **125**, 2909–2935.

Nitta, T., 1987: Convective activities in the tropical western Pacific and their impact on the Northern Hemisphere summer circulation. *J. Meteor. Soc. Japan*, **65**, 373–390.

Ramage, C. S., 1968: Role of a tropical "maritime continent" in the atmospheric circulation. *Mon. Wea. Rev.*, **96**, 365–369.

Rayner, N. A., D. E. Parker, E. B. Horton, C. K. Folland, L. V. Alexander, D. P. Rowell, E. C. Kent, and A. Kaplan, 2003: Global analyses of sea surface temperature, sea ice, and night marine air temperature since the late nineteenth century. *J. Geophys. Res.*, **108**, 4407, doi: 10.1029/2002JD002670.

Rodwell, M. J., and B. J. Hoskins, 1996: Monsoons and the dynamics of deserts. *Quart. J. Roy. Meteor. Soc.*, **122**, 1385–1404.

Saji, N. H., and T. Yamagata, 2003: Possible impacts of Indian Ocean Dipole mode events on global climate. *Climate. Res.*, **25**, 151–169.

Saji, N. H., B. N. Goswami, P. N. Vinayachandran, and T. Yamagata, 1999: A dipole mode in the tropical Indian Ocean. *Nature*, **401**, 360–363.

Schneider, U., A. Becker, P. Finger, A. Meyer-Christoffer, B. Rudolf, and M. Ziese, 2011: *GPCC full data reanalysis version 6.0 at 1.0°: Monthly land-surface precipitation from rain-gauges built on GTS-based and historic data*. Global Precipitation Climatology Centre (GPCC). Berlin, Germany, doi:10.5676/DWD_GPCC/FD_M_V6_100.

Simpson, G. C., 1921: The origin of the south-west monsoon. *Nature*, **107**, 154.

Tao, S.-Y., and L.-X. Chen, 1987: A review of recent research on the East Asian summer monsoon in China. *Monsoon Meteorology*. Chang, C.-P., and T. N. Krishnamurti (eds.), Oxford University Press, 60–92.

Taschetto, A. S., C. C. Ummenhofer, A. S. Gupta, and M. H. England, 2009: Effect of anomalous warming in the central Pacific on the Australian monsoon. *Geophys.*

Res. Lett., **36**, L12704, doi:10.1029/2009GL038416.

Teng, D. G., X. F. Liu, Z. X. Zhang, and S. A. Wu, 2005: Interannual variation of Australian high and its effect on Asia-Australia monsoon circulation system in summer. *J. Nanjing Inst. Meteor.*, **28**, 86–92 (in Chinese).

Torrence, C., and P. J. Webster, 1999: Interdecadal changes in the ENSO–monsoon system. *J. Climate*, **12**, 2679–2690.

Wang, B., and H. Rui, 1990: Dynamics of the coupled moist Kelvin–Rossby wave on an equatorial β-plane. *J. Atmos. Sci.*, **47**, 397–413.

Wang, B., R. Wu, and K.-M. Lau, 2001: Interannual variability of the Asian summer monsoon: Contrasts between the Indian and the western North Pacific–East Asian monsoons. *J. Climate*, **14**, 4073–4090.

Wang, B., R. Wu, and T. Li, 2003: Atmosphere-warm ocean interaction and its impacts on Asian-Australian monsoon variation. *J. Climate*, **16**, 1195–1211.

Wang, B., Z. Wu, J. Li, J. Liu, C.-P. Chang, Y. Ding, and G. Wu, 2008: How to measure the strength of the East Asian summer monsoon. *J. Climate*, **21**, 4449–4463.

Wang, C., Y. Bo, R. Li, and H. Bao, 2016: Impacts of the Asia-Australia dipole and ENSO on climate variability in the Asia-Australia region. *Int. J. Climatol.*, **36**, 4202–4212.

Wang, H., and K. Fan, 2013: Recent changes in the East Asian monsoon. *Chin. J. Atmos. Sci.*, **37**, 313–318 (in Chinese).

Wang, M., Z. Guan, and D. Jin, 2018: Two new sea surface temperature anomalies indices for capturing the eastern and central equatorial Pacific type El Niño-Southern Oscillation events during boreal summer. *Int. J. Climatol.*, **38**, 4066–4076.

Webster, P. J., 1983: Mechanisms of monsoon low-frequency variability: Surface hydrological effects. *J. Atmos. Sci.*, **40**, 2110–2124.

Webster, P. J., and S. Yang, 1992: Monsoon and ENSO: Selectively interactive systems. *Quart. J. Roy. Meteor. Soc.*, **118**, 877–926.

Wu, R., and B. Wang, 2002: A contrast of the East Asian summer monsoon–ENSO relationship between 1962–77 and 1978–93. *J. Climate*, **15**, 3266–3279.

Wu, R. G., Z. Wen, S. Yang, and Y. Li, 2010: An interdecadal change in southern China summer rainfall around 1992/93. *J. Climate*, **23**, 2389–2403.

Wu, R. G., S. Yang, Z. Wen, G. Huang, and K. Hu, 2012: Interdecadal change in the relationship of southern China summer rainfall with tropical Indo-Pacific SST. *Theor. Appl. Climatol.*, **108**, 119–133.

Wu, R. G., G. Huang, Z. Du, and K. Hu, 2014: Cross-season relation of the South China Sea precipitation variability between winter and summer. *Climate Dyn.*, **43**, 193–207.

Xie, S.-P., and S. G. H. Philander, 1994: A coupled ocean-atmosphere model of relevance to the ITCZ in the eastern Pacific. *Tellus A*, **46**, 340–350.

Xie, S.-P., Y. Okumura, T. Miyama, and A. Timmermann, 2008: Influences of Atlantic climate change on the tropical Pacific via the Central American Isthmus. *J. Climate*, **21**, 3914–3928.

Xie, S.-P., K. Hu, J. Hafner, H. Tokinaga, Y. Du, G. Huang, and T. Sanpe, 2009: Indian Ocean capacitor effect on Indo–Western Pacific climate during the summer following El Niño. *J. Climate*, **22**, 730–747.

Xu, J., and J. C. L. Chan, 2001: The role of the Asian–Australian monsoon system in the onset time of El Niño events. *J. Climate*, **14**, 418–433.

Xu, Q., and Z.-Y. Guan, 2017a: Interdecadal change of diabatic forcing over key region of the Maritime Continent and its possible relations with East Asian summer monsoon anomalies. *J. Trop. Meteor.*, **25**, 54–62 (in Chinese).

Xu, Q., and Z.-Y. Guan, 2017b: Interannual variability of summertime outgoing longwave radiation over the Maritime Continent in relation to East Asian summer monsoon anomalies. *J. Meteor. Res.*, **31**, 665–677.

Yang, X., Z.-Y. Guan, and B.-L. Zhu, 2007: Role of Indian Ocean Dipole events in the influence of ENSO on the summer rainfall and temperature in China. *J. Nanjing Inst. Meteor.*, **30**, 170–177 (in Chinese).

Yu, B., and Z.-Y. Guan, 2009: Simulated structural changes of Asian summer monsoon circulation in association with Indian Ocean dipole SSTA. *Trans. Atmos. Sci.*, **32**, 765–775 (in Chinese).

Yuan, Y., H. Yang, W. Zhou, and C. Li, 2008: Influences of the Indian Ocean dipole on the Asian summer monsoon in the following year. *Int. J. Climatol.*, **28**, 1849–1859.

Zhang, P.-B., Z.-Y. Guan, and J.-X. Cai, 2010a: Impacts of interannual variations of Australian high on the summer temperature in China by SVD analysis. *Trans. Atmos. Sci.*, **33**, 58–66 (in Chinese).

Zhang, P.-B., Z.-Y. Guan, M.-N. Sun, and S.-Y. Cao, 2010b: Possible impacts of the interannual variability of the Australian high on summertime rainfall in China as revealed by the SVD analysis. *J. Meteor. Res.*, **68**, 908–917 (in Chinese).

Zhang, P.-B., Z.-Y. Guan, L. Liu, Y. Jiang, and H.-E. Jing, 2016: Possible influence of SST anomaly in maritime continent on summer climate of china in association with variations of Australian high. *Plateau Meteor.*, **35**, 188–197 (in Chinese).

Zhu, C., B. Wang, W. Qian, and B. Zhang, 2012: Recent weakening of northern East Asian summer monsoon: A possible response to global warming. *Geophys. Res. Lett.*, **39**, L09701, doi:10.1029/2012GL051155.

Zhu, J., H. Liao, and J. Li, 2012: Increases in aerosol concentrations over eastern China due to the decadal–scale weakening of the East Asian summer monsoon. *Geophys. Res. Lett.*, **39**, L09809, doi:10.1029/2012GL051428.